Electronic Supplementary Information (ESI)

Branched Aramid Nanofiber-Polyaniline Electrodes for Structural Energy Storage

Paraskevi Flouda,[a] Alexander H. Quinn,[b] Anish G. Patel,[b] Dimitrios Loufakis,[a] Dimitris C. Lagoudas,[a,c] and Jodie L. Lutkenhaus[a,b,*]

[a]Department of Materials Science and Engineering, Texas A&M University, College Station, TX 77843, United States

[b]Artie McFerrin Department of Chemical Engineering, Texas A&M University, College Station, TX 77843, United States

[c]Department of Aerospace Engineering, Texas A&M University, College Station, TX 77843, United States

*Correspondence: jodie.lutkenhaus@tamu.edu

Preparation of initial PANI composites (Table S1): PANI and PANI:poly(2-acrylamido-2-methyl-1-propanesulfonic acid) (PAAMPSA) complexes were prepared following prior reports from our group.[1-3] Initially, dispersions of PANI and PANI:PAAMPSA (1 mg/ml) in water/DMSO were directly vacuum filtered using a Nylon filter paper (pore size: 0.2 μm and diameter: 47 mm). BANF-containing composites were fabricated by mixing and stirring for 2 h desired amounts of PANI or PANI:PAAMPSA dispersions with BANF dispersions (1 mg/ml) in water/DMSO followed by vacuum filtration. Layered PANI/BANF composites were fabricated using sequential vacuum filtration. More specifically, desired amounts of BANFs/DMSO (1 mg/ml) were filtered to form thin films of BANFs. Subsequently, PANI/water (1 mg/ml) mixtures were filtered through the BANF premade membrane. Finally, composites containing PANI:PAAMPSA, 10 wt% BANFs, and 10 wt% of a third component (b-PEI, MWCNT-COOH, or GO) were fabricated by directly mixing and stirring for 2 h dispersions of the components (1 mg/ml) in water followed by vacuum filtration. GO dispersions (1 mg/ml) in water were prepared following previous reports using the modified Hummers' method.[4, 5] All composites were washed with a 1M HCl solution and dried under vacuum at 60 ^{o}C for 3 days. Composites containing MWCNT-COOH and GO were thermally reduced at 200 ^{o}C for 2 h under vacuum. The total mass of the composites was kept constant at ~20 mg.

Table S1 Failed fabrication attempts for PANI-containing free-standing electrodes.

Attempt #	Sample	Approach	Issue
1	PANI: 100 wt%	Vacuum filtration of PANI dispersion in water	Cracked film 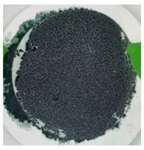
2	PANI: 90 wt% BANF: 10 wt%	Vacuum filtration of PANI/BANF dispersion in DMSO	PANI is soluble in DMSO, thus not captured by filter paper
3	PANI: 90 wt% BANF 10 wt%	Vacuum filtration of PANI/BANF dispersion in water	Cracked film 
4	PANI 90 wt% BANF 10 wt%	Layer by layer vacuum filtration: 1st layer BANF/DMSO 2nd layer PANI/water	Poor electrochemical performance (specific capacitance of <10 F/g)
5	PANI:PAAMPSA: 100 wt%	Vacuum filtration of PANI:PAAMPSA dispersion in water	Cracked film 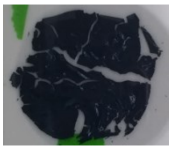
6	PANI:PAAMPSA: 90 wt% BANF: 10 wt%	Vacuum filtration of PANI:PAAMPSA/BANF dispersion in DMSO	PANI:PAAMPSA is soluble in DMSO, thus not captured by filter paper
7	PANI:PAAMPSA: 90 wt% BANF: 10 wt%	Vacuum filtration of PANI:PAAMPSA/BANF dispersion in water	Cracked film 
8	PANI:PAAMPSA: 80 wt% BANF: 10 wt% b-PEI: 10 wt %	Vacuum filtration of PANI:PAAMPSA/BANF/b-PEI dispersion in water	Cracked film 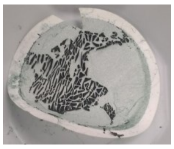
9	PANI:PAAMPSA: 80 wt% BANF: 10 wt% MWCNT-COOH: 10 wt%	Vacuum filtration of PANI:PAAMPSA/BANF/MWCNT-COOH dispersion in water	Poor electrochemical performance (specific capacitance of <10 F/g)
10	PANI:PAAMPSA: 80 wt% BANF: 10 wt% GO: 10 wt%	Vacuum filtration of PANI:PAAMPSA/BANF/GO dispersion in water	Poor electrochemical performance (specific capacitance of <80 F/g)

Table S2 Composition of composite films using the gravimetric method.

	PANI (wt%)	BANF (wt%)	SWCNT (wt%)	PANI/CNT	BANF/CNT
BANF	-	100	-	-	-
PANI/BANF	15	85	-	-	-
PANI/BANF/7 wt% CNT	13	80	7	1.86	11.4
PANI/BANF/12 wt% CNT	15	73	12	1.25	6.1
PANI/BANF/22 wt% CNT	14	64	22	0.63	2.9
PANI/BANF/29 wt% CNT	15	56	29	0.51	1.9
BANF/CNT	-	86	14	-	6.1
PANI/CNT	12	-	88	0.44	-

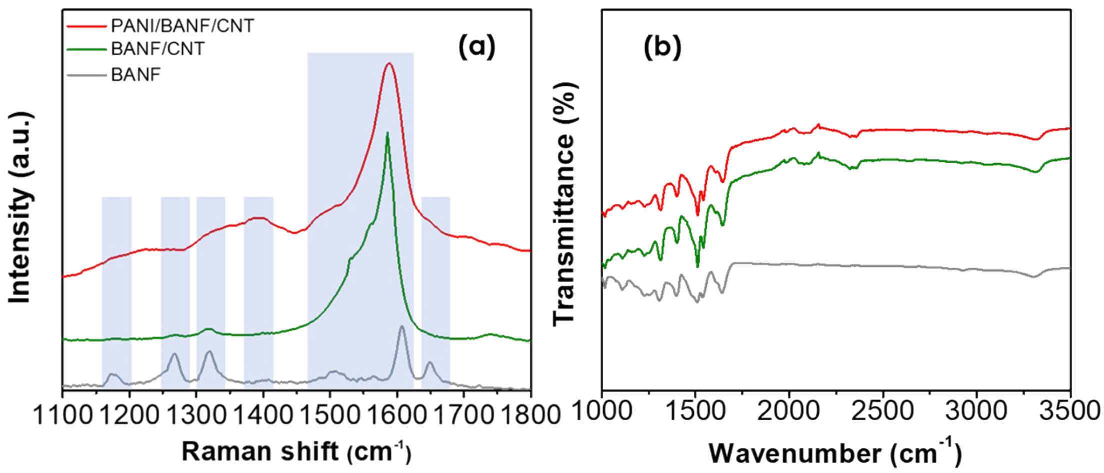

Fig. S1 (a) Raman and (b) FT-IR spectra for BANF, BANF/CNT, and PANI/BANF/CNT. Legend in panel (a) applies also in panel (b). The shaded regions refer to peaks of interest (Table S3).

Table S3 Raman spectroscopy for BANF, BANF/CNT, and PANI/BANF/CNT.

Raman shift [cm^{-1}]	BANF	BANF/CNT	PANI/BANF/CNT
1176	C=C stretching	C=C stretching	C=C stretching/C-H bending
1267	C=C stretching	C=C stretching	C=C stretching
1321	C-H in plane bending	C-H in plane bending	C-H in plane bending
1331	-	-	C-N stretching
1496	-	-	C=N stretching
1508	C=C stretching	C=C stretching	C=C stretching
1564	N-H bending/C-N stretching	N-H bending/C-N stretching	N-H bending/C-N stretching
1588	-	G-band	G-band
1608	C=C stretching	C=C stretching	C=C stretching
1650	C=O stretching	C=O stretching	C=O stretching

Table S4 FT-IR/ATR spectroscopy for BANF, BANF/CNT, and PANI/BANF/CNT.

Wavenumber [cm^{-1}]	BANF	BANF/CNT	PANI/BANF/CNT
1173	C-H in-plane deformation	C-H in-plane deformation	C-H in-plane deformation/ N=Q=N stretching
1318	C-N stretching of secondary aromatic amines	C-N stretching of secondary aromatic amines	C-N stretching of secondary aromatic amines
1490	C-H bending	C-H bending	C-H bending /N-B-N stretching
1515	C=C stretching	C=C stretching	C=C stretching
1545	N-H deformation and C-N stretching coupled modes	N-H deformation and C-N stretching coupled modes	N-H deformation and C-N stretching coupled modes
1645	C=O stretching	C=O stretching	C=O stretching
3300	N-H stretching	N-H stretching	N-H stretching

* B represents benzenoid and Q quinoid moieties in PANI

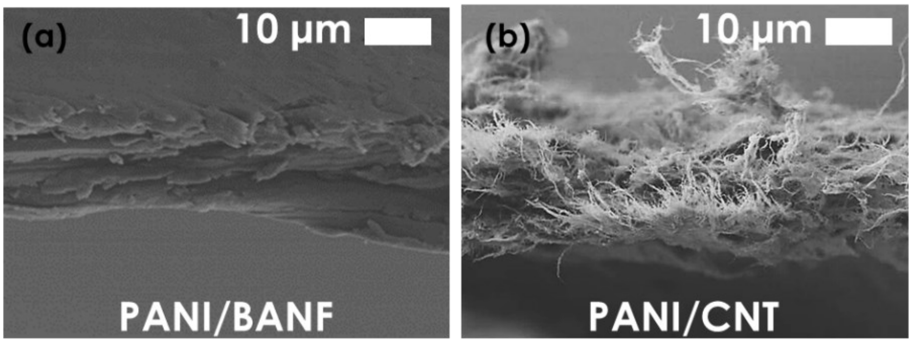

Fig. S2 Cross-sectional SEM images for (a) PANI/BANF and (b) PANI/CNT.

Table S5 Mechanical and electrical properties.

Sample	Young's modulus [GPa]	Ultimate strength [MPa]	Ultimate strain [%]	Toughness [kJ/m^3]	Conductivity [S/cm]
BANF	3 ± 0.1	138 ± 5.3	8.5 ± 0.2	7100 ± 175	-
PANI/BANF	5.4 ± 0.6	58 ± 1.4	1.9 ± 0.4	770 ± 270	0.0014 ± 0.0001
BANF/CNT	2.5 ± 0.2	64 ± 6	5.4 ± 0.9	1900 ± 350	0.13 ± 0.02
PANI/CNT	1.8 ± 0.3	18.2 ± 3.1	1.2 ± 0.1	136 ± 25	28 ± 1.4
PANI/BANF/7 wt% CNT	4.6 ± 0.4	48 ± 4.5	1.8 ± 0.2	508 ± 20	0.21 ± 0.03
PANI/BANF/12 wt% CNT	4 ± 0.5	40 ± 4	1.7 ± 0.2	430 ± 40	2.5 ± 0.4
PANI/BANF/22 wt% CNT	1.5 ± 0.3	14.3 ± 1.5	1.4 ± 0.1	96 ± 27	2.8 ± 0.2
PANI/BANF/29 wt% CNT	1.4 ± 0.2	10.8 ± 1.7	1.2 ± 0.2	81 ± 20	3.0 ± 0.2

Table S6 Ashby plot data for PANI-containing composites.

Sample	Young's modulus [GPa]	Ultimate strength [MPa]	Conductivity [S/cm]	Film fabrication method
2-layer PANI/ANF[6]	3.4	150	19.3	Layer by layer filtration
PANI/PC[7]	0.8	28	0.01	Pressurized powder
PANI/BC[8]	5.6	95.7	0.05	In-situ polymerization on premade BC films
PANI/CS[9]	1.7	32.3	7.69×10^{-7}	Drop-casting
PANI/ANF VF[10]	1.3	50	0.001	Vacuum filtration
PANI/CNT[11]	1.9	9.9	1.9	Vacuum filtration
PANI/BANF/12 wt% CNT (this work)	4 ± 0.5	40 ± 4	2.3 ± 0.6	Vacuum filtration
PANI/BANF (this work)	5.4 ± 0.6	58 ± 1.4	0.0014 ± 0.0001	Vacuum filtration
BANF/CNT (this work)	2.5 ± 0.2	64 ± 6	0.13 ± 0.02	Vacuum filtration
PANI/CNT (this work)	1.8 ± 0.3	18.2 ± 3.1	28 ± 1.4	Vacuum filtration

Table S7 Specific capacitance (based on active mass: PANI and CNT) at varying scan rates from cyclic voltammetry.

Scan rate [V/s]	PANI/BANF [F/g]	BANF/CNT [F/g]	PANI/CNT [F/g]	PANI/BANF/12 wt% CNT [F/g]
0.001	7.5 ± 0.3	9.8 ± 0.2	299.1 ± 1.2	245.4 ± 2.6
0.005	6.0 ± 0.2	6.6 ± 0.3	278.7 ± 0.5	207.2 ± 1.4
0.01	4.1 ± 0.3	5.8 ± 0.1	250.2 ± 0.9	180.8 ± 4.1
0.02	2.3 ± 0.1	5.7 ± 0.5	220.1 ± 2.3	159.3 ± 0.9
0.05	1.3 ± 0.2	5.9 ± 0.4	172.3 ± 3.5	131.4 ± 1.3
0.1	0.8 ± 0.1	6.0 ± 0.5	130.2 ± 0.8	108.2 ± 3.7

Table S8 Cycling stability for 1,000 cycles at 0.5 A/g from galvanostatic charge/discharge test (based on active mass: PANI and CNT).

cycle #	PANI/BANF [F/g]	BANF/CNT [F/g]	PANI/CNT [F/g]	PANI/BANF/12 wt% CNT [F/g]
1	7 ± 0.9	19.7 ± 1.3	259.3 ± 4.2	206.9 ± 2.1
50	5.5 ± 1.2	16.0 ± 2.1	252.3 ± 4.6	181.2 ± 3.7
100	3.2 ± 0.5	14.3 ± 0.9	251.4 ± 5.3	166.3 ± 6.2
200	2.3 ± 0.6	12.1 ± 0.7	246.3 ± 3.2	154.4 ± 5.8
300	-	9.7 ± 3.2	244.7 ± 5.8	148.5 ± 4.6
400	-	7.4 ± 0.9	240.2 ± 6.2	145.5 ± 3.2
500	-	3.1 ± 0.6	236.1 ± 4.1	139.7 ± 3.3
600	-	-	233.5 ± 4.0	133.6 ± 3.9
700	-	-	232.9 ± 3.8	130.7 ± 3.1
800	-	-	231.3 ± 2.1	127.7 ± 3.7
1000	-	-	229.7 ± 2.7	121.8 ± 5.1

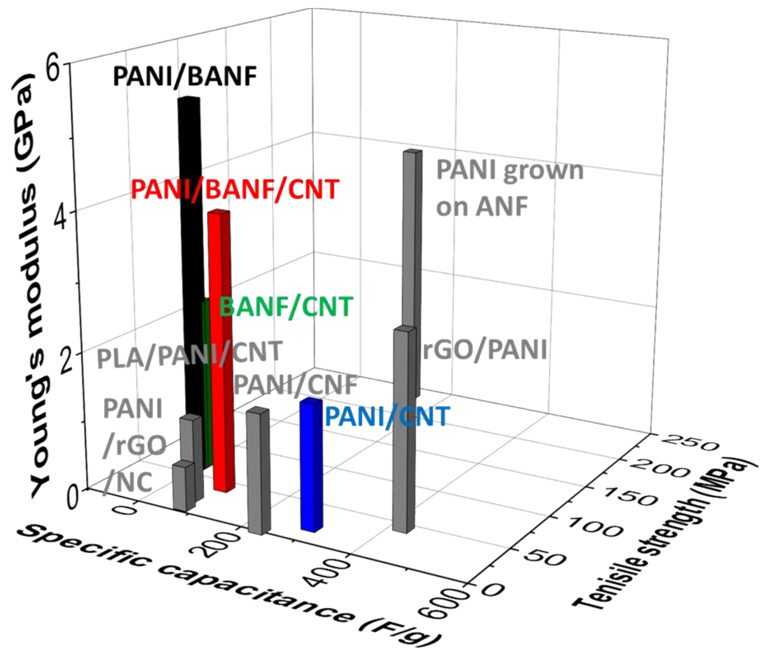

Fig. S3 Ashby plot of Young's modulus *vs*. specific capacitance *vs.* tensile strength for PANI-containing free-standing supercapacitor electrodes. Specific capacitance values were calculated per total electrode mass.

Table S9 Ashby plot data for PANI-containing supercapacitor electrodes.

Sample	Young's modulus [GPa]	Ultimate strength [MPa]	Specific capacitance [F/g], based on active mass	Specific capacitance [F/g], based on total mass	Film fabrication method
rGO/PANI[12]	2.8	43	424.4	424.4	Vacuum filtration
PANI/CNF[13]	1.7	0.5	-	234.0	In-situ polymerization on free standing CNF films
PANI/NC[14]	6.6	12.4	421.5	-	Vacuum filtration
PANI/rGO/NC[15]	0.64	5.8	-	79.7	Vacuum filtration
PLA/CNT/PANI[16]	1.2	18.7	510.3	70	In-situ polymerization on free standing PLA/CNT films
PANI grown on ANF[17]	4	233.3	168	138	In-situ polymerization on free standing ANF films
PANI/BANF/12 wt% CNT (this work)	4 ± 0.5	40 ± 4	245.4 ± 2.6	90.6 ± 1.0	Vacuum filtration
PANI/BANF (this work)	5.4 ± 0.6	58 ± 1.4	7.5 ± 0.3	1.3 ± 0.1	Vacuum filtration
BANF/CNT (this work)	2.5 ± 0.2	64 ± 6	9.8 ± 0.2	1.6 ± 0.1	Vacuum filtration
PANI/CNT (this work)	1.8 ± 0.3	18.2 ± 3.1	299.1 ± 1.2	299.1 ± 1.2	Vacuum filtration

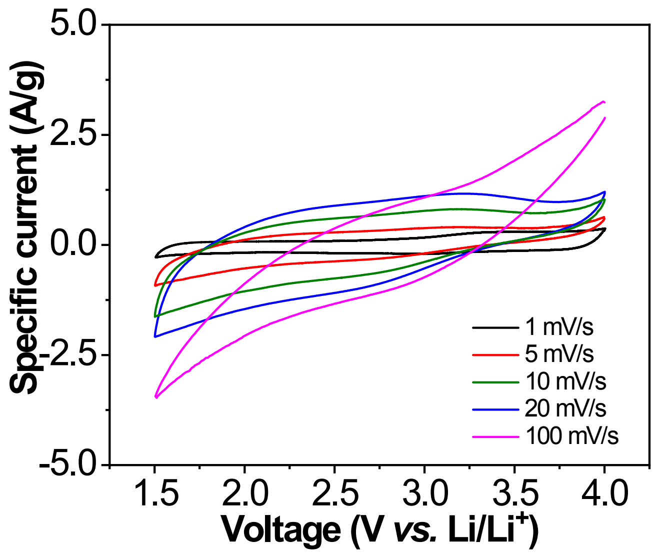

Fig. S4 Cyclic voltammograms for PANI/BANF/12 wt% CNT cathodes in a lithium metal half-cell at varying scan rates (1-100 mV/s) in a 1.5 to 4 V *vs.* Li/Li^+ voltage range.

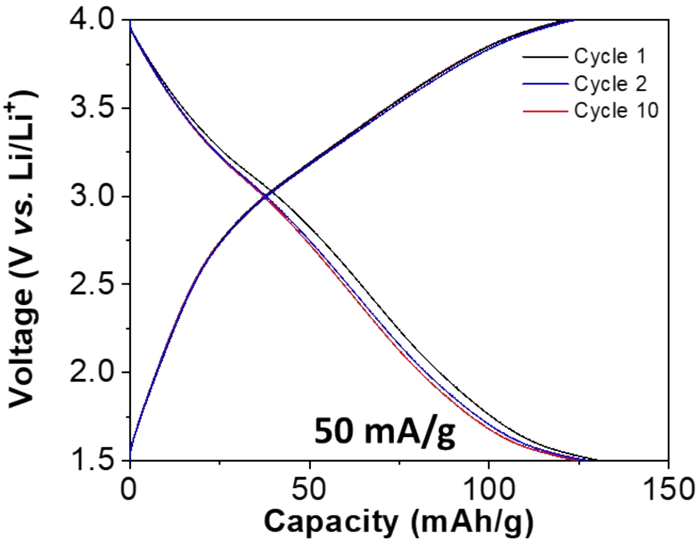

Fig. S5 Galvanostatic charge-discharge curves at 50 mA/g for the 1st, 2nd, and 10th cycle for a PANI/BANF/12 wt% CNT cathode in a lithium metal half-cell.

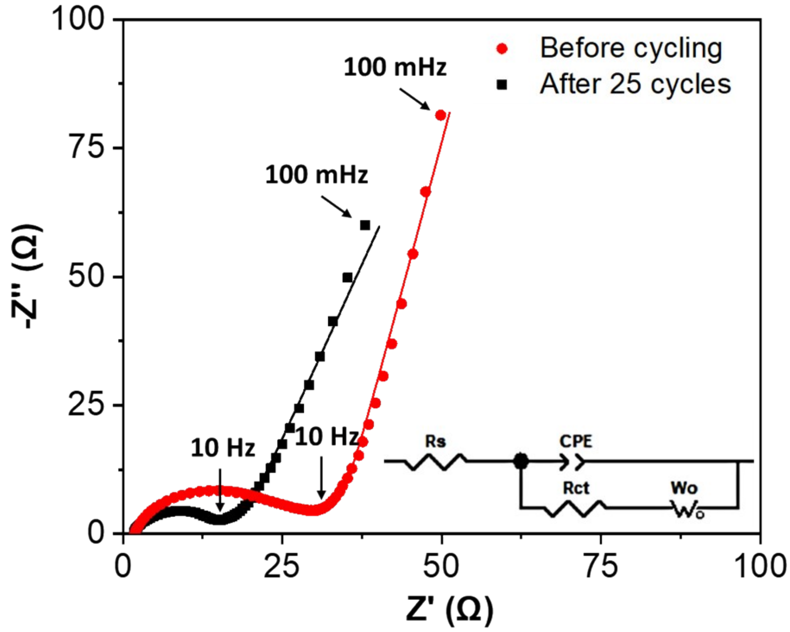

Fig. S6 Nyquist plot of PANI/BANF/12 wt% CNT cathode obtained by performing EIS before cycling and after 25 cycles. The inset shows the equivalent circuit used to model the data. EIS was conducted at 3.3 V *vs.* Li/Li^+ with a 5 mV amplitude and a frequency range of 1 MHz - 100 mHz.

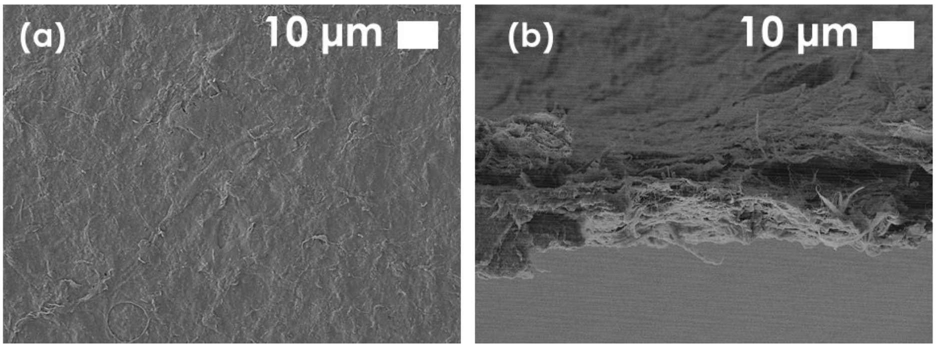

Fig. S7 SEM images for PANI/BANF/12 wt% CNT cathodes after 200 charge-discharge cycles at 50 mA/g of the (a) surface and (b) cross-section.

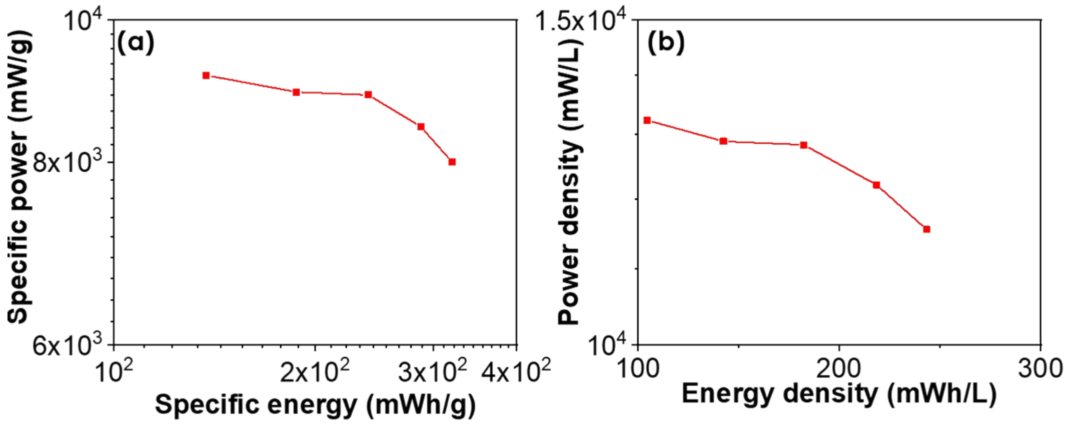

Fig. S8 (a) Specific power *vs.* specific energy and (b) power density *vs.* energy density for PANI/BANF/12 wt% CNT cathodes in a lithium metal half-cell.

Table S10 Comparison of gravimetric capacity against other PANI containing battery electrodes.

Sample	Specific capacity [mAh/g], based on PANI mass	Specific capacity [mAh/g], based on total mass	Specific current/C-rate and electrolyte	Mechanical properties	Electrode fabrication method
PANI/MXene[18]	188	144.7	100 mA/g and 1 M $LiClO_4$ in PC	Not reported	Layer by layer
PANI/rGO[3]	524	461	100 mA/g and 0.5 M $LiClO_4$ in PC	Not reported	Layer by layer
PANI/SWCNT aerogels[19]	181	140	60 mA/g and 1 M $LiPF_6$ in EC:DEC	Not reported	Supercritical drying of hydrogel
PANI/MWCNTs[20]	Not reported	122.8	20 mA/g and 1 M $LiPF_6$ in EC:DMC	Not reported	Doctor blading
PANI/Polyoxometalate nanofibers[21]	Not reported	183.4	0.1 C and 1 M $LiPF_6$ in EC:DEC	Not reported	Doctor blading
PANI/BANF/12 wt% CNT (this work)	128 ± 5	25.6 ± 1	50 mA/g (0.33 C) and 1 M $LiPF_6$ in EC:DEC:DMC	See Table S5	Vacuum filtration

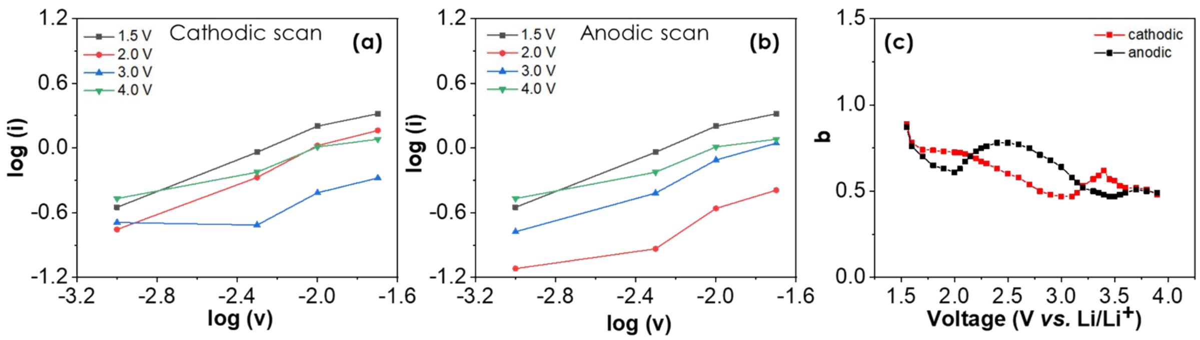

Fig. S9 Plot of log(i) *vs.* log(v) for (a) cathodic and (b) anodic scans in cyclic voltammetry for PANI/BANF/12 wt% CNT cathodes. (c) Plot of b-value *vs.* potential (V *vs.* Li/Li^+) as calculated from $\log(i) = b\cdot\log(v) + \log(a)$.

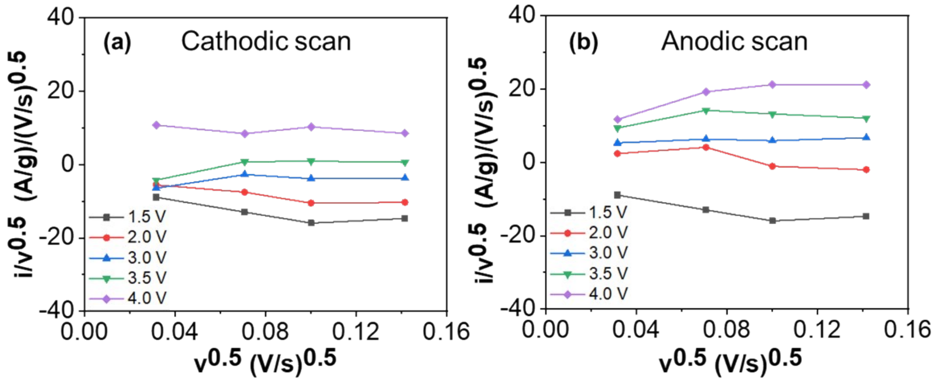

Fig. S10 Graphs of $i/v^{0.5}$ *vs.* $v^{0.5}$ for (a) cathodic and (b) anodic scans for PANI/BANF/12 wt% CNT cathodes.

References

1. J.-W. Jeon, J. O'Neal, L. Shao and J. L. Lutkenhaus, *ACS Applied Materials & Interfaces*, 2013, **5**, 10127-10136.
2. J.-W. Jeon, Y. Ma, J. F. Mike, L. Shao, P. B. Balbuena and J. L. Lutkenhaus, *Physical Chemistry Chemical Physics*, 2013, **15**, 9654-9662.
3. J.-W. Jeon, S. R. Kwon and J. L. Lutkenhaus, *Journal of Materials Chemistry A*, 2015, **3**, 3757-3767.
4. W. S. Hummers and R. E. Offeman, *Journal of the American Chemical Society*, 1958, **80**, 1339-1339.
5. P. Flouda, J. Yun, D. Loufakis, S. A. Shah, M. J. Green, D. C. Lagoudas and J. L. Lutkenhaus, *Sustainable Energy & Fuels*, 2020, **4**, 2301-2308.
6. J. Lyu, X. Zhao, X. Hou, Y. Zhang, T. Li and Y. Yan, *Compos. Sci. Technol.*, 2017, **149**, 159-165.
7. B. H. Jeon, S. Kim, M. H. Choi and I. J. Chung, *Synth. Met.*, 1999, **104**, 95-100.
8. W. Hu, S. Chen, Z. Yang, L. Liu and H. Wang, *The Journal of Physical Chemistry B*, 2011, **115**, 8453-8457.
9. T. Thanpitcha, A. Sirivat, A. M. Jamieson and R. Rujiravanit, *Carbohydr. Polym.*, 2006, **64**, 560-568.
10. X. Han, L. Lv, D. Yu, X. Wu and C. Li, *ACS Applied Materials & Interfaces*, 2019, **11**, 3466-3473.
11. F. M. Blighe, D. Diamond, J. N. Coleman and E. Lahiff, *Carbon*, 2012, **50**, 1447-1454.
12. R. Hu, J. Zhao, G. Zhu and J. Zheng, *Electrochim. Acta*, 2018, **261**, 151-159.
13. M. Yanilmaz, M. Dirican, A. M. Asiri and X. Zhang, *Journal of Energy Storage*, 2019, **24**, 100766.
14. W. Zheng, R. Lv, B. Na, H. Liu, T. Jin and D. Yuan, *Journal of Materials Chemistry A*, 2017, **5**, 12969-12976.
15. H. H. Hsu, A. Khosrozadeh, B. Li, G. Luo, M. Xing and W. Zhong, *ACS Sustainable Chemistry & Engineering*, 2019, **7**, 4766-4776.
16. Q. Wang, H. Wang, P. Du, J. Liu, D. Liu and P. Liu, *Electrochim. Acta*, 2019, **294**, 312-324.
17. Q. Yin, H. Jia, A. Mohamed, Q. Ji and L. Hong, *Nanoscale*, 2020, **12**, 5507-5520.
18. J. Yun, I. Echols, P. Flouda, S. Wang, A. Easley, X. Zhao, Z. Tan, E. Prehn, G. Zi, M. Radovic, M. J. Green and J. L. Lutkenhaus, *ACS Applied Materials & Interfaces*, 2019, DOI: 10.1021/acsami.9b16692.
19. D. Ge, L. Yang, A. Honglawan, J. Li and S. Yang, *Chemistry of Materials*, 2014, **26**, 1678-1685.

20. B.-L. He, B. Dong, W. Wang and H.-L. Li, *Materials Chemistry and Physics*, 2009, **114**, 371-375.
21. H. Yang, T. Song, L. Liu, A. Devadoss, F. Xia, H. Han, H. Park, W. Sigmund, K. Kwon and U. Paik, *The Journal of Physical Chemistry C*, 2013, **117**, 17376-17381.